Supporting Information

A combined SAXS/WAXS/XAFS set-up capable of observing concurrent changes across the nano-to-micrometer size range in inorganic solid crystallization processes

Andrew M. Beale[†], Ad M. J. van der Eerden[†], Simon D. M. Jacques[‡], Olivier Leynaud[‡], Matthew G. O'Brien[‡], Florian Meneau[√], Sergei Nikitenko[√], Wim Bras[√], Bert M. Weckhuysen[†]*

[†] Inorganic Chemistry and Catalysis, Utrecht University, Sorbonnelaan 16, 3584 CA Utrecht, The Netherlands

[‡] Department of Chemistry, University College London, 20 Gordon Street, London WC1H 0AJ, UK.

[√] Netherlands Organisation for Scientific Research (NWO), DUBBLE@ESRF, Grenoble, F-38043, France

Experimental section

Sample preparation

The following chemicals were used in the synthesis in accordance with similar methods previously described to prepare AlPO-5 or MeAPO-5 (where Me = transition metal) materials:[1] a gel was prepared containing 0.131 g $Zn(NO_3)_3.4H_2O$ (Acros Organics 99%), 69 ml H_3PO_4 (Acros Organics 85 wt. % in water), 1.04 ml Triethylamine (Acros Organics 99%) and 0.658 g pseudoboehmite Alumina CATAPAL B 73.6 wt. % Al_2O_3 (Sasol North America Inc.). The white, amorphous precursor gel used in the experiments had the stoichiometry $Zn_xAl_{1-x}PO_4$ where x = 0.05 (zinc content ~ 2.5 wt. %) and a pH ≈ 3.5.

Setup

Data collection was carried out on station BM26A of the ESRF (Grenoble, France) using a Si(111) double crystal fast scanning monochromator. Two vertically focusing Pt and Si-coated mirrors were used to remove the higher harmonics. An ion chamber (for I_o) and translational photodiode (I_t) were used for recording XAFS data whereas SAXS/WAXS data were recorded simultaneously using a 1D quadrant gas-filled detector positioned at a distance of 1.8 m from the sample (SAXS) and position sensitive

curved gaseous INEL CPS 590 detector (WAXS) after the photodiode was removed at the end of the XAFS scan.[2] WAXS and EXAFS data acquisition was controlled using the sequence mode of the EXAFS program developed at Daresbury laboratory. SAXS data was collected on a separate computer using the locally developed SAXS GUI program. A total cycle time of 5 minutes was employed to collect the data (3 minutes for XAS from 9.465 - 10.30 keV and 2 minutes for SAXS/WAXS (at a wavelength of 1.3098 Å) which includes a 10 s dead time to move the monochromator back to the start position and a further 10 s to move the I_t photodiode into/out of the beam). However potentially the time resolution could be as fast as 30 s per spectra/pattern although this will be dependent on the wavelength(s) used, the sample thickness/density and the extent to which sacrifices in data quality can be tolerated. The program cycle used is better illustrated in Figure S1. The figure is essentially a plot of the energy of the beam focused on the sample vs. the temperature of the *in situ* cell with time. The plot clearly illustrates the regions and energies at which combined SAXS/WAXS data (*ca.* 9.465 keV ≈ 1.3098 Å corresponding to scattering q vectors in the range $0.3 < q < 2$ nm^{-1}) and XAFS data (9.465 - 10.30 keV) were recorded. Since a ramp rate of 1°C/min. was employed to heat up the sample, the time from the beginning of the experiment can be determined by subtracting the starting temperature (30°C) from all subsequent temperatures. Due to the small amount of material formed during the reaction, the beam size was reduced to a minimum size (height 150 μm x 3 mm width) and positioned in the lower part of the cell aperture.
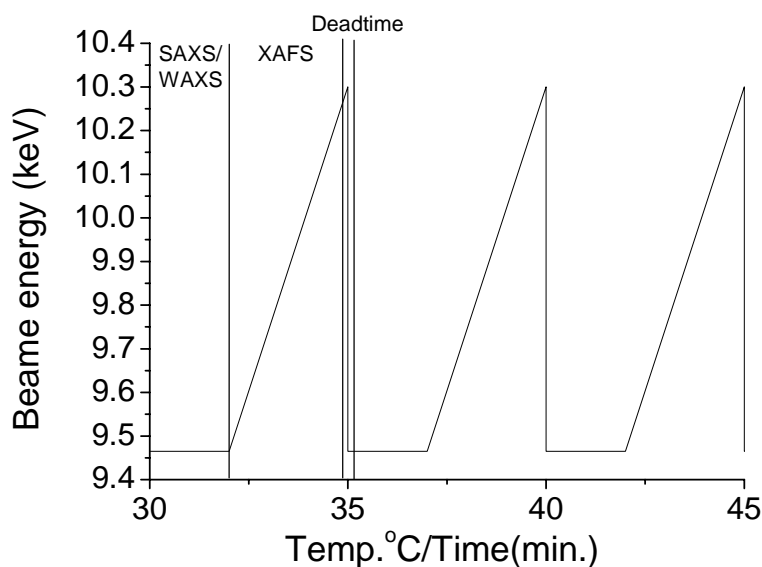
Figure S1. Timing/temperature vs. energy sequence employed for the acquisition of combined SAXS/WAXS/XAFS data during the hydrothermal crystallization of ZnAPO-34.

Data Processing

<u>SAXS</u>

For the calibration of the SAXS detector, a silver behenate reference sample was used.[3] Although data were collected over a k range $0.3 < q < 2$ nm^{-1}, due to the limitations imposed by the sample and the cell, analysis could only be performed over the range range $0.3 < q < 0.9$ nm^{-1}. However previous measurements performed by some of us on CoAPO-5 samples showed, that despite these restrictions, it is possible to identify global changes that occurred in the amorphous gel before the onset of crystallization.[4] Unfortunately the quality of the data prevented any further analysis (such as a Generalized Indirect Fourier Transformation analysis) to identify particle size distributions, structure and possible interactions. This is obviously a common problem when obtaining time resolved data.

WAXS

In order to accommodate the furnace and various detector arrays, the sample position with respect to the curved INEL WAXS detector had to be offset from the middle of the 2θ circle. This geometric offset meant that the detector response was non-linear over the 2θ range in which WAXS data was recorded. In order to correct for this problem a pattern from a NIST silicon standard in which the d-spacing for a number of reflections (e.g. 111, 220, 311….) are well known was recorded and the differences between the 2θ values observed vs. 2θ values expected approximated using a 2nd order polynomial function.

Peak broadening: Peak broadening remains much less of a problem when collecting synchrotron radiation powder diffraction data since it is often well collimated. This results in narrow peaks possessing a simple pseudo-Voigt shape. However broadening due to detector limitations is still a problem making reliable information regarding crystallite sizes difficult to determine. In order to reduce this problem it is possible to empirically determine an approximate peak broadening effect using a crystalline sample in which the crystallite size has been determined using other techniques. This value can then be incorporated into a particle size estimation using the well-known Sherrer equation (Equation 1). In this case we used a fully crystallized AlPO-5 sample, which did not appear to suffer significantly from strain or stacking faults and where the crystallite size had been determined using SEM, to estimate approximately the degree of 'instrument broadening'.

$$t = \frac{0.9\,\lambda}{B\cos\theta}$$

Equation 1

Where:

t = crystallite size

0.9 = typical shape factor of the average crystallite

λ = X-ray wavelength

B = Bragg peak width (minus the instrument peak broadening)

θ = Diffraction angle

Analysis of diffraction data

The evolution of diffraction peak intensity as a function of time can be used to derive valuable information on the kinetics and the mechanism involved in the crystallization process. The intensity was determined by fitting the −111 Bragg peaks with a Gaussian function and measuring the corresponding areas that are then converted to the extent of reaction (α), scaled from 0 to 1, using the relationship α (t)= $I_{hkl}(t)/I_{hkl}(max)$, where $I_{hkl}(t)$ is the area of a given peak at time t, and $I_{hkl}(max)$ the maximum area of this peak. Kinetic data and information both on the dimensionality and the process of crystallisation can be derived from the Avrami-Erofe'ev[5-8] expression that is widely used to model phase transitions and crystal growth in solid-state chemistry using the extent of the reaction, α, to time t using the relationship:

$$\alpha = 1 - \exp[-(k(t-t_0))^n]$$

where t is the induction time, k the rate constant, and *n* is the Avrami exponent. The exponent *n*, can be used in most cases to deduce information about the rate of nucleation and the mechanism of nuclei growth.[9] Common values of *n* range from n = 0.5 to n = 4. Previous work has demonstrated the relevance of this equation in modelling a variety of solid-state reactions.[10] A Sharp-Hancock plot (ln [-ln(1-α)] vs. ln (time)) shown in Figure S2 is typically used to obtain the gradient *n* and intercept *n* ln k.[11]
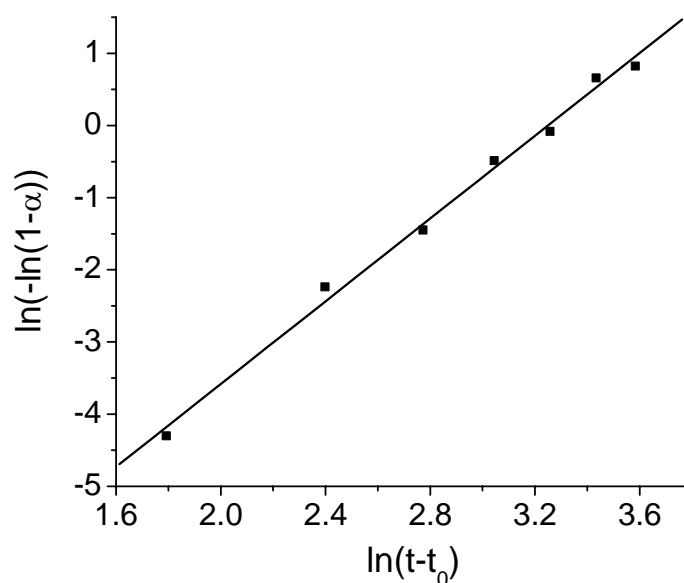
Figure S2. Sharp-Hancock plot for the formation of ZnAPO-34 over the range $0.10 < \alpha < 0.8$.

XAFS

XAFS data were processed using the programs developed at Daresbury laboratory, *i.e.*, EXCALIB for converting the raw data to energy vs. absorption coefficient, EXBROOK to obtain the normalized XANES part of the spectra (normalized to give an edge jump of 1) and for pre and post-edge background subtraction to extract the EXAFS and EXCURV98 to perform a least-squares iterative fitting of the EXAFS data.[12] EXAFS refinements were carried out on k^3-weighted spectra plotted over a k-range of 3-10 Å^{-1} considering only single scattering paths. Only a shell of oxygen near neighbors was considered in the fitting process. Due to problems with material moving inside the sample cell (which we note is typical for hydrothermal samples) fluctuations in sample density caused the amplitude of the XAFS signal to occasionally drop resulting in unphysical values for the average Zn-O first coordination sphere. In order to correct for this problem the coordination number was fixed to 4.0 (which we justify since the average Zn-O distance remained *ca.* 1.94 Å typical of tetrahedral Zn^{2+})[12] in the fitting process. A best fit of the data (in k-space) was determined by minimizing the EXAFS R-factor (a meaningful indication of the quality of fit of the EXAFS data as a percentage).

Since these data were obtained in time-resolved mode typical R-factors were between 28 – 35 %. An example fit for data recorded at 40°C is given below in Figure S3.
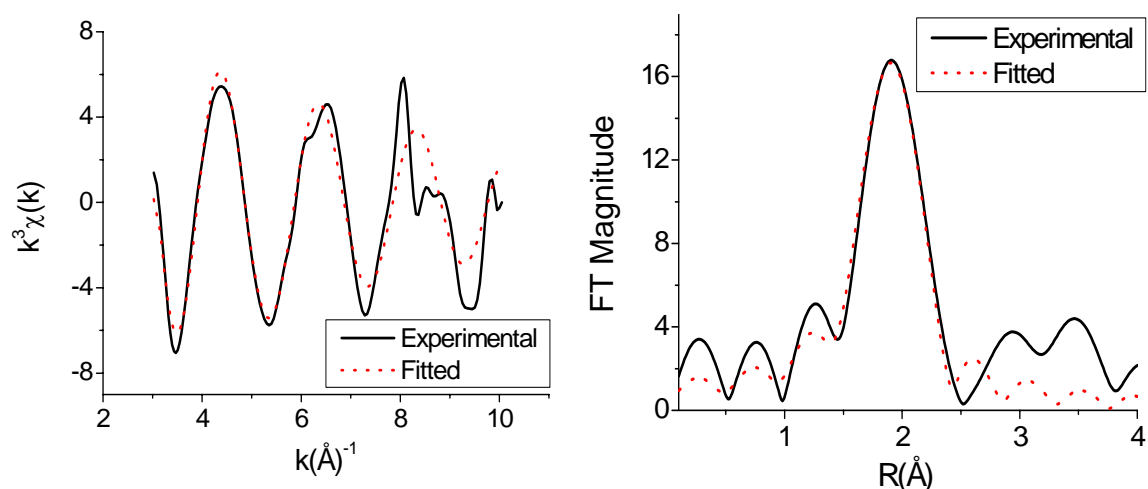
Figure S3. Fitted Zn K-edge EXAFS (left hand side) and associated fourier transform (FT) recorded at 40°C during the heating of the zinc aluminophosphate gel to form ZnAPO-34.

Perspective

Possibilities for the integration of additional spectroscopic techniques

This article has demonstrated clearly that by observing the attenuation by the sample of a 'straight-through' X-ray beam it is possible to obtain information on the various atomic, nano- and micro-domain changes that occurred during the crystallization of a microporous material. However, it is conceivable that other non X-ray based methods might also be coupled in addition (space allowing) to or in place of one/two of the X-ray techniques to yield further insight into the formation of such materials. Two of the more obvious and appropriate techniques that could be used with such a set-up include diffuse reflectance UV-Visible and/or Raman spectroscopy. Both techniques have been sufficiently developed so that they may be employed either within (using fiber-optic microprobes) or external to the hydrothermal reactor cell and it has been shown that they can provide additional insights into microporous material self-assembly processes.[4,14] In particular Raman spectroscopy, in addition to information regarding the formation of structural units, can also provide insight into the behavior of the templating species and

potentially to the identification of important solvent interactions.[15] This suggests that when Raman Spectroscopy can be combined with the X-ray based methods, a more complete understanding of the crystallization process might be possible.

References

(1) Chen, J. S.; Sankar, G.; Thomas, J. M.; Xu, R. R.; Greaves, G. N.; Waller, D. *Chem. Mater.* **1992**, *4*, 1373.

(2) Bras, W. *J. Macromol. Sci. Phys.* **1998,** *37*, 557.

(3) (a) Blanton, T. N.; Barnes, C. L.; Lelental, M. *J. Appl. Cryst.* **2000**, *33*, 172. (b) Huang, T. C.; Toraya, H.; Blanton, T. N.; Wu, Y. *J. Appl. Cryst.* **1993**, *26*, 180.

(4) Grandjean, D.; Beale, A. M.; Petukhov, A. V.; Weckhuysen, B. M. *J. Am. Chem. Soc.* **2005**, *127*, 14454.

(5) Erofe'ev, B. V. *C. R. Dokl. Acad. Sci. URSS* **1946**, *52*, 511.

(6) Avrami, M. *J. Chem. Phys.* **1939**, *7*, 1103.

(7) Avrami, M. *J. Chem. Phys.* **1940**, *8*, 212.

(8) Avrami, M. *J. Chem. Phys.* **1941**, *9*, 177.

(9) (a) Hulbert, F. *J. Brit. Ceram. Soc.* **1969**, *6*, 11. (b) Grizzetti, R.; Artioli, G. *Microp. Mesop.* **2002**, *54*, 105.

(10) (a) Fogg, A. M.; Price, S. J.; Francis, R. J.; O'Brien, S.; O'Hare, D. *J. Mater. Chem.* **2000**, *10*, 2355. (b) Milanesio, M.; Artioli, G.; Gualtieri, A. F.; Palin, L.; Lamberti, C. *J. Am. Chem. Soc.* **2003**, *125*, 14549.

(11) Hancock, J. H.; Sharp, J. D. *J. Amer. Ceram. Soc.* **1972**, *55*, 74.

(12) Binsted, N.; Campbell, J. W.; Gurman, S. J.; Stephenson, P. C. *EXAFS Analysis Programs,* Daresbury Laboratory, Warrington, 1991.

(13) Cooley, R. F. R.; Reed, J. S. *J. Am. Ceram. Soc.* **1972**, *55,* 395.

(14) (a) Weckhuysen, B. M.; Baetens, D.; Schoonheydt, R. A. *Angew. Chem. Int. Ed.* **2000**, *39*, 3419. (b) Tinnemans, S. J.; Mesu, J. G.; Kervinen, K.; Visser, T.; Nijhuis, T. A.; Beale, A. M.; Keller, D. E.; van der Eerden, A. M. J.; Weckhuysen, B. M. *Catal. Today* **2006**, *113*, 3. (c) Grunwaldt, J. D.; Wandeler, R.; Baiker, A. *Catal. Rev. Sci. Eng.* **2003**, *45*, 1.

(15) (a) Xiong, G.; Yu, Y.; Feng, Z. C.; Xin, Q.; Xiao, F. S.; Li, C. *Microp. Mesop.* **2001**, *42*, 317. (b) Pastore, H. O.; Coluccia, S.; Marchese, L. *Annu. Rev. Mater. Res.* **2005**, *25*, 351. (c) Kecht, J.; Mihailova, B.; Karaghiosoff, A.; Mintova, S.; Bein T. *Langmuir*, **2004**, *20*, 5271.